6-2001

Parity Violation in Neutron Resonances of Antimony and Iodine

Y Matsuda
Kyoto University

J D. Bowman
Los Alamos National Laboratory

Bret E. Crawford
Gettysburg College

See next page for additional authors

Matsuda, Y., Bowman, J. D., Crawford, B. E., Delheij, P. J., Haseyama, T., Knudsen, J. N., Lowie, L. Y., Masaike, A., Masuda, Y., Mitchell, G. E., Penttila, S. I., Postma, H., Roberson, N. R., Seestrom, S. J., Sharapov, E. I., Stephenson, S., Yen, Y.F., & Yuan, V. W. (2001). Parity violation in neutron resonances of antimony and iodine. Physical Review C, 64(015501).

Parity Violation in Neutron Resonances of Antimony and Iodine

Abstract

Parity violation in p-wave neutron resonances of ^{121}Sb, ^{123}Sb, and ^{127}I has been measured by transmission of a longitudinally polarized neutron beam through natural antimony and iodine targets. The measurements were performed at the pulsed spallation neutron source of the Los Alamos Neutron Science Center. Five statistically significant parity violation effects were observed in ^{121}Sb, one effect in ^{123}Sb, and seven effects in ^{127}I. The weak interaction rms matrix elements and the corresponding spreading widths were determined.

Disciplines

Atomic, Molecular and Optical Physics | Physics

Authors

Y Matsuda, J D. Bowman, Bret E. Crawford, P P J. Delheij, T Haseyama, J N. Knudsen, L Y. Lowie, A Masaike, G E. Mitchell, S I. Penttila, H Postma, N R. Roberson, S J. Seestrom, E I. Sharapov, Sharon L. Stephenson, Y-F Yen, and V W. Yuan

Parity violation in neutron resonances of antimony and iodine

Y. Matsuda,[1,*] J. D. Bowman,[2] B. E. Crawford,[3,†] P. P. J. Delheij,[4] T. Haseyama,[1,‡] J. N. Knudsen,[2] L. Y. Lowie,[5,§] A. Masaike,[1,‖] Y. Masuda,[6] G. E. Mitchell,[5] S. I. Penttilä,[2] H. Postma,[7] N. R. Roberson,[3] S. J. Seestrom,[2] E. I. Sharapov,[8] S. L. Stephenson,[5,¶] Y.-F. Yen,[2,**] and V. W. Yuan[2]

[1]*Physics Department, Kyoto University, Kyoto 606-01, Japan*
[2]*Los Alamos National Laboratory, Los Alamos, New Mexico 87545*
[3]*Duke University, Durham, North Carolina 27708*
and Triangle Universities Nuclear Laboratory, Durham, North Carolina 27708-0308
[4]*TRIUMF, Vancouver, British Columbia, Canada V6T 2A3*
[5]*North Carolina State University, Raleigh, North Carolina 27695-8202*
and Triangle Universities Nuclear Laboratory, Durham, North Carolina 27708-0308
[6]*National Laboratory of High Energy Physics, Tsukuba-shi 305, Japan*
[7]*Delft University of Technology, IRI, 2629 JB Delft, The Netherlands*
[8]*Joint Institute for Nuclear Research, RU-141980 Dubna, Russia*

(Received 26 March 2001; published 15 June 2001)

Parity violation in *p*-wave neutron resonances of ^{121}Sb, ^{123}Sb, and ^{127}I has been measured by transmission of a longitudinally polarized neutron beam through natural antimony and iodine targets. The measurements were performed at the pulsed spallation neutron source of the Los Alamos Neutron Science Center. Five statistically significant parity violation effects were observed in ^{121}Sb, one effect in ^{123}Sb, and seven effects in ^{127}I. The weak interaction rms matrix elements and the corresponding spreading widths were determined.

DOI: 10.1103/PhysRevC.64.015501 PACS number(s): 24.80.+y, 25.40.Ny, 27.60.+j, 11.30.Er

I. INTRODUCTION

Following the discovery of very large parity violation for neutron resonances in heavy nuclei by Alfimenkov *et al.* [1], the time reversal invariance and parity at low energies (TRIPLE) collaboration was formed to study parity violation in compound nuclei. The high neutron flux available at the Manuel Lujan Jr. Neutron Scattering Center (MLNSC) at the Los Alamos Neutron Science Center (LANSCE) was very well suited for these experiments. A statistical ansatz was adopted: the compound nucleus is considered to be a chaotic system and the symmetry-breaking matrix elements are random variables. In this approach the result of a parity violation experiment is the root-mean-square symmetry-breaking matrix element, which is obtained from a set of longitudinal asymmetries $\{p\}_E$ measured for many resonances. The crucial point is that the value of the rms matrix element can be obtained without detailed information about the wave functions. For a particular resonance at energy E, the asymmetry p is defined by

$$\sigma^{\pm}(E) = \sigma_{\mathrm{p}}(E)(1 \pm p), \tag{1}$$

where $\sigma^{\pm}(E)$ is the neutron cross section for the + and − neutron helicity states, and $\sigma_{\mathrm{p}}(E)$ is the *p*-wave resonance cross section for unpolarized neutrons. Results from the early measurements by our group are discussed in reviews by Bowman *et al.* [2], Frankle *et al.* [3], and Flambaum and Gribakin [4]. After the initial measurements we improved the experimental system, repeated and improved the early measurements, and carried out experiments with many additional targets. The most recent reviews are by Mitchell, Bowman, and Weidenmüller [5] and by Mitchell *et al.* [6].

In practice the parity violation measurements are feasible only near a maximum of the *p*-wave neutron strength function. The TRIPLE measurements with ^{232}Th [7] and ^{238}U [8] were near the maximum of the $4p$ neutron strength function, and gave no information concerning any mass dependence of the effective nucleon-nucleus weak interaction. Our attention next turned to the $A=110$ mass region, where the $3p$ neutron strength function maximum is located. We performed measurements on a number of targets in this region and results have been published for several nuclides: ^{93}Nb [9], ^{103}Rh [10], ^{107,109}Ag [11], ^{113}Cd [12], ^{115}In [13], and ^{133}Cs [14]. Parity nonconserving (PNC) effects were observed for all but one of the odd mass targets that we studied near the $3p$ neutron strength function maximum. However, for targets with nonzero spin the analysis of the parity violation data is complicated. As discussed below, it is important to have spectroscopic information (including spins) for the *s*- and *p*-wave resonances. In the absence of such spectroscopic information one can average over the various possibilities, but this averaging often introduces a large uncertainty into the value for the rms PNC matrix element.

In the present paper we report our PNC study on antimony and iodine. Iodine is monoisotopic. Natural antimony is 57.3% ^{121}Sb and 42.7% ^{123}Sb. We took advantage of the approximately equal abundance and moderate level densities

*Present address: Institute of Physical and Chemical Research (RIKEN), Saitama 351-0198, Japan.
†Present address: Dickinson College, Carlisle, PA 17013.
‡Present address: Institute of Chemical Research, Kyoto University, Kyoto 611-0011, Japan.
§Present address: McKinsey and Company, Atlanta, GA 30303.
‖Present address: Fukui University of Technology, 3-6-1 Gakuen, Fukui-shi 910-8505, Japan.
¶Present address: Gettysburgh College, Gettysburg, PA 17325.
**Present address: Wake Forest University School of Medicine, Winston-Salem, NC 27157.

to study both isotopes simultaneously. A similar approach for silver (which has an approximately equal abundance of ^{107}Ag and ^{109}Ag) worked very well [11]. One complication was that an additional measurement was required to assign newly observed resonances in natural antimony to a specific isotope. This measurement was performed with an enriched target (99.48% ^{121}Sb) and a γ-ray detector array [15].

In Sec. II the experimental methods for the parity violation measurements are described. The experimental data and the analysis to obtain the longitudinal asymmetries are discussed in Sec. III. The extraction of the PNC matrix elements and the weak spreading widths is described in Sec. IV. The results and conclusions are given in Sec. V.

II. EXPERIMENTAL METHOD

Transmission measurements of the PNC asymmetries p were performed at the MLNSC pulsed neutron source at LANSCE. This spallation source is described by Lisowski *et al.* [16]. The apparatus developed by the TRIPLE Collaboration to measure p is described in a number of papers, including the original experimental layout [17], the neutron monitor [18], the polarizer [19], the spin flipper [20], and the neutron detector [21]. The layout of the polarized neutron beam line for the present PNC experiments is given in Ref. [8]. The measurements were performed on flight path 2, which views a gadolinium-poisoned water moderator and has a cadmium/boron liner to reduce the number of low-energy neutrons emerging in the tail of the neutron pulse. After the moderator the neutrons are collimated to a 10-cm diameter beam inside a 4-m thick biological shield. The neutrons then pass through a ^{3}He/^{4}He ion chamber system [18] that acts as a flux monitor. The neutron flux is measured by the monitor for each neutron burst, and these measurements are used to normalize the detector rates. Next, the neutrons pass through a polarized-proton spin filter [19] where neutrons with one of the two helicity states are preferentially scattered out of the beam, leaving a beam of longitudinally polarized neutrons (with polarization $f_n \simeq 70\%$). Fast neutron spin reversal (every 10 s) was accomplished by passing the neutron beam through a spin reversal device consisting of a system of magnetic fields [20]. In addition to the frequent and fast spin reversals, the neutron spin direction was also changed by reversing the polarization direction of the proton spin filter. Since this latter process takes several hours, it was only performed approximately every 2 days. For the experimental data on antimony and iodine, approximately half of the data were taken with ''positive'' direction of the spin filter and about half with ''negative'' direction.

The PNC effects in antimony and iodine were measured by transmitting the neutron beam through samples located at the downstream part of the spin flipper. The cylindrical sample of natural antimony had an areal density of 3.67×10^{23} atoms/cm^2 of ^{121}Sb and 2.74×10^{23} atoms/cm^2 of ^{123}Sb. The natural crystalline iodine target had an areal density of 7.24×10^{23} atoms/cm^2. The ^{10}B-loaded liquid scintillation neutron detector [21] was located 56.7 m from the neutron source. This 55-cell segmented detector can handle instantaneous counting rates up to 9 MHz per cell with a dead time of about 20 ns. The detector has an efficiency of 95%, 85%, and 71% at neutron energies of 10 eV, 100 eV, and 1000 eV, respectively. The neutron mean capture time in the detector is (416 ± 5) ns. The data acquisition process is initiated with each proton burst. The detector signals are linearly summed and filtered. An analog-to-digital converter transient recorder digitally samples the summed detector signal 8192 times in intervals determined by the filtering time. The 8192 words are added, as a ''pass,'' to a summation memory for 200 beam bursts before being stored. The data from 160 passes form a 30-min ''run'' for the data analysis.

III. EXPERIMENTAL DATA

Several new resonances were observed in the transmission spectrum of the natural antimony target. The assignment of these new resonances to a particular isotope of antimony was achieved using the γ-ray detector array and a sample enriched to 99.48% ^{121}Sb. Most of the new resonances belong to ^{121}Sb—the level density for ^{121}Sb is more than twice as large as the level density for ^{123}Sb. Resonance parameters were determined by analysis of the data summed over both helicity states. Background and dead time corrections were applied as described by Crawford *et al.* [8]. The shape analysis was performed with the code FITXS [22], which was written specifically to analyze the time-of-flight (TOF) spectra measured by the TRIPLE Collaboration. The multilevel, multichannel formalism of Reich and Moore [23] was used for the neutron cross sections, which were convoluted with the TOF resolution function studied in detail by Crawford *et al.* [8]. The final fitting function is written as

$$\mathcal{F}_t(t) = \left[B_t(t) \otimes \left(\frac{\alpha}{E^{0.96}} e^{-n\sigma_D(t)} \right) \right] + \sum_{i=0}^{3} \frac{a_i}{t^i}, \qquad (2)$$

where $\sigma_D(t)$ is the Doppler-broadened total cross section, $B_t(t)$ is the instrumental response function (which includes line broadening due to the initial width of the pulsed beam, neutron moderation, finite TOF channel width, and mean time for neutron capture in the detector), $\alpha/E^{0.96}$ is the energy dependent neutron flux, and the second term represents a polynomial fit to the background. (The symbol $\otimes$ indicates a convolution.) Details of the fitting procedures are given by Crawford *et al.* [8]. From this analysis the neutron resonance energies and $g\Gamma_n$ widths were obtained.

A TOF spectrum for the natural antimony target in the energy region 150 to 210 eV is shown in Fig. 1. The resonances that are readily observable are all s-wave resonances. A sample multilevel fit to two p-wave resonances in antimony near 260 eV is shown on an expanded scale in Fig. 2. These resonances are both in ^{121}Sb. A TOF spectrum for the iodine target is shown in Fig. 3 in the energy region 150–210 eV. Again the s-wave resonances dominate. A fit for two iodine p-wave resonances near 135 eV is shown on an expanded scale in Fig. 4.

Due to normalization issues, the precision of our measured resonance parameters is no better than the published values. Therefore for the parity violation analyses we used the energies, neutron widths, and spins for the s-wave resonances from evaluated nuclear data file (ENDF) evaluations

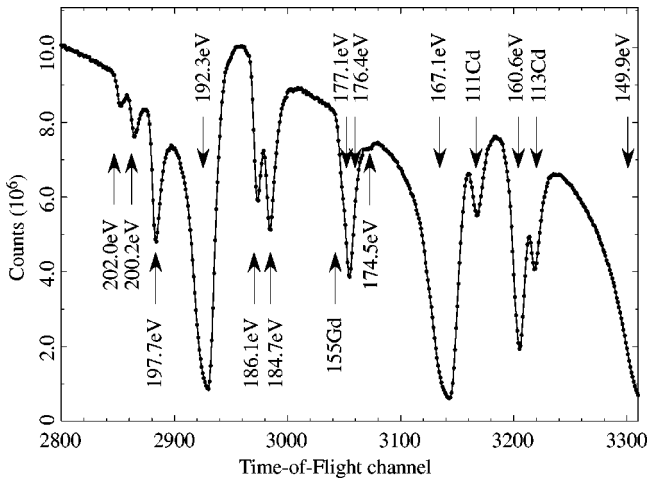

FIG. 1. Neutron time-of-flight spectrum for transmission in natural antimony in the energy range 150–210 eV. The resonances indicated are all *s*-wave resonances.

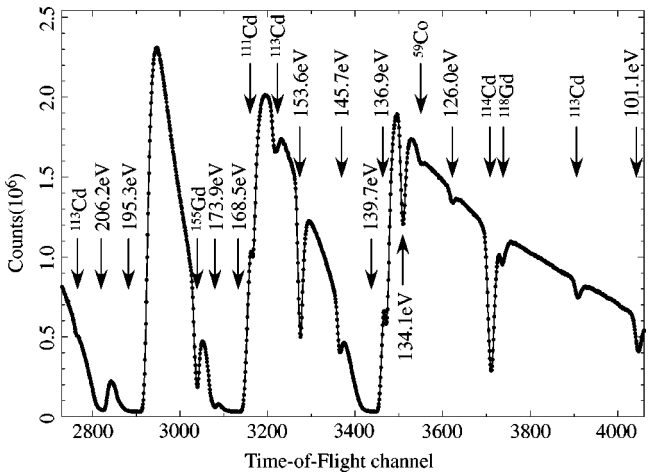

FIG. 3. Neutron time-of-flight spectrum for transmission in iodine in the energy range 100–220 eV. The resonances indicated are all *s*-wave resonances.

[24] for iodine and from Japanese evaluated nuclear data library (JENDL) evaluations [25] for antimony. We used our measured values for the *p*-wave resonances.

After determining the resonance parameters and fixing them, the parameters $(f_n p)^+$ and $(f_n p)^-$ in equations

$$\sigma^{\pm}_{pf_n} = \sigma_p[1 + (f_n p)^{\pm}] \tag{3}$$

were determined separately for the + and − helicity TOF spectra. The data were fit on a run-by-run basis. Here $\sigma^{\pm}_{pf_n}$ is the experimental neutron cross section for the + and − neutron helicity states (which is dependent on the beam polarization), and f_n is the absolute value of the neutron beam polarization. The value of f_n was determined in a separate study of the well-known longitudinal asymmetry of the 0.75-eV resonance in lanthanum [26]. Because the f_n value is very nearly the same for the + and − helicities, the quantities $(f_n p)^+$ and $(f_n p)^-$ should differ only by a sign, although statistical and systematic uncertainties may introduce further differences. The asymmetry *p* defined by Eq. (1) was calculated as

$$p = \frac{[(f_n p)^+ - (f_n p)^-]}{f_n[2 + (f_n p)^+ + (f_n p)^-]}. \tag{4}$$

The PNC amplification parameters are $A_{pJ} = \sqrt{\Sigma 4(g\Gamma^s_{nJ}/g\Gamma^p_{nJ})/(E_{sJ} - E_{pJ})^2}$, where the sum is over the *s*-wave resonances (see Sec. IV). These parameters are called amplification factors or enhancement factors, and depend on knowledge of the spin *J* because the weak interaction only mixes *p*- and *s*-wave resonances with the same spin *J*. The resonance parameters, enhancement factors, and longitudinal

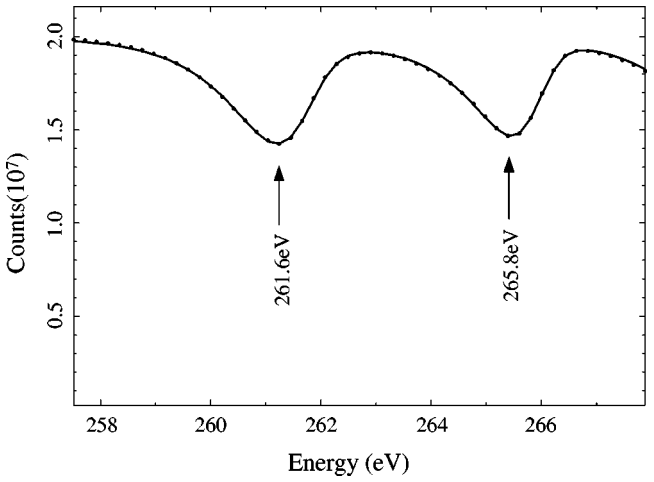

FIG. 2. Neutron time-of-flight spectrum for transmission in natural antimony shown on an expanded energy scale near 260 eV. The solid line represents the fit obtained with the analysis code FITXS. Note that the asymmetric line shapes of the two *p*-wave resonances are well reproduced.

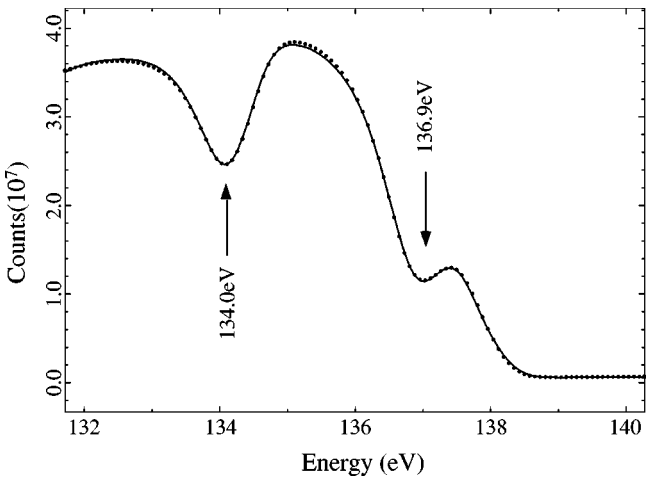

FIG. 4. Neutron time-of-flight spectrum for transmission in iodine shown on an expanded energy scale near 135 eV. The solid line represents the fit obtained with the code FITXS. The shapes of the two *p*-wave resonances are well reproduced, although they are distorted by the presence of a nearby large *s*-wave resonance.

TABLE I. Resonance parameters and PNC asymmetries for *p*-wave resonances of ^{121}Sb.

E (eV)	$g\Gamma_n$ (meV)	A_2 [a] (eV^{-1})	A_3 [a] (eV^{-1})	p (%)	$\lvert p\rvert/\Delta p$
37.9	0.0085±0.0009	2.8	4.8	0.018±0.016	1.1
55.21	0.014±0.002	10.2	2.3	−0.133±0.018	7.3
92.10 [b]	0.017±0.002	2.2	20.2	-0.51±0.05	10.2
110.7 [b]	0.037±0.005	17.6	3.1	2.15±0.06	35.8
141.2 [b]	0.0081±0.0008	18.4	12.5	1.26±0.12	10.5
174.5 [b]	0.0054±0.0005	10.7	5.3	0.045±0.033	1.4
176.9	0.043±0.004			0.03±0.07	0.4
184.7	0.126±0.012			−0.051±0.033	1.5
200.3 [b]	0.0054±0.0005			−0.029±0.076	0.4
228.6	0.044±0.004			−0.072±0.075	1.0
235.9	0.019±0.002			−0.05±0.16	0.3
245.9	0.235±0.022			0.017±0.045	0.4
249.0	0.128±0.012			0.138±0.052	2.7
261.6	0.181±0.018			−0.029±0.036	0.8
265.8	0.167±0.017			0.080±0.048	1.7
270.0	0.208±0.021			0.179±0.046	3.9
274.8	0.153±0.015			0.128±0.050	2.6

[a]Values above 174.5 eV are not listed; see text for explanation.
[b]New resonances.

asymmetries are listed for ^{121}Sb in Table I and for ^{123}Sb in Table II (see also Figs. 5 and 6). Since the spins of the *p*-wave resonances are unknown, there are two possible A_J values corresponding to the two possible spins for which the levels can mix and show parity violation. The resonance parameters, enhancement factors, and longitudinal asymmetries are listed for ^{127}I in Table III.

IV. ANALYSIS

The details of the analysis to obtain the weak matrix elements and spreading widths from the PNC cross section asymmetries are given by Bowman *et al.* [27]. Specific applications have been described in a number of our previous papers, e.g., our study of PNC effects in silver [11] illustrates the analysis for $I\neq 0$ targets. The essential argument is that the observed PNC effect in the *p*-wave resonance in question is due to contributions from a number of neighboring *s*-wave resonances. Since there are several mixing matrix elements and one measured asymmetry, one cannot obtain the individual matrix elements. Assuming that the weak matrix elements connecting the opposite parity states are random variables leads to the result that the longitudinal asymmetry is also a random variable. From the distribution of the asymmetries one can infer the variance M^2 of the individual matrix elements $V_{\nu\mu}$—the mean square matrix element of the PNC interaction. The details of the analysis depend on knowledge of the spectroscopic parameters. The essence of our approach to the likelihood analysis is to include all available spectroscopic information and to average over remaining unknowns. The net result is that more information reduces the uncertainty in the rms value of the weak matrix element.

In general the observed asymmetry for a given *p*-wave level μ has contributions from several *s*-wave levels ν, and the PNC asymmetry is

$$p_\mu = 2\sum_\nu \frac{V_{\nu\mu}}{E_\nu - E_\mu}\frac{g_\nu g_{\mu_{1/2}}}{\Gamma_{\mu_n}}, \tag{5}$$

where $g_{\mu_{1/2}}$ and g_ν are the neutron decay amplitudes of levels μ and ν ($g_\mu^2 = g_{\mu_{1/2}}^2 + g_{\mu_{3/2}}^2 \equiv \Gamma_{\mu_n}$ and $g_\nu^2 \equiv \Gamma_{\nu_n}$), E_μ and E_ν are the corresponding resonance energies, and $V_{\nu\mu}$ is the matrix element of the PNC interaction between levels μ and ν.

TABLE II. Resonance parameters and PNC asymmetries for *p*-wave resonances of ^{123}Sb.

E (eV)	$g\Gamma_n$ (meV)	A_2 (eV^{-1})	A_3 (eV^{-1})	p (%)	$\lvert p\rvert/\Delta p$
176.4	0.176±0.017	1.5	0.9	−0.076±0.042	1.8
186.1	0.154±0.015	4.2	0.8	−0.012±0.035	0.3
197.7	0.243±0.024	3.3	0.6	−0.02±0.035	0.6
202.0 [a]	0.160±0.016	2.4	0.7	−0.46±0.12	3.8
225.2	0.160±0.016	1.3	1.1	−0.014±0.045	0.3

[a]New resonance.

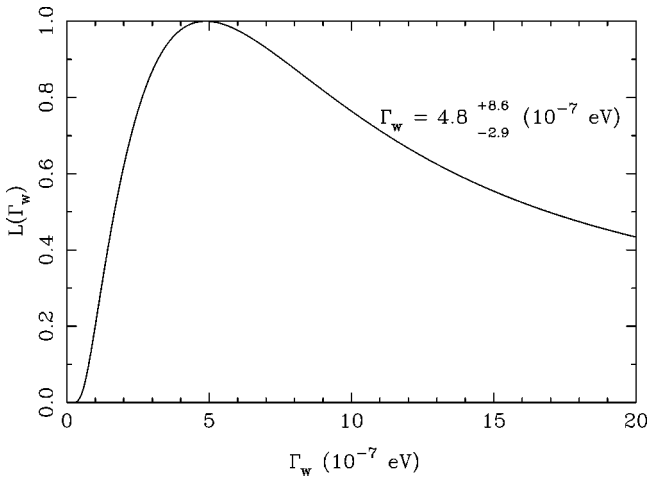

FIG. 5. Likelihood plot for ^{121}Sb. A total of 17 *p*-wave resonances were analyzed and five statistically significant PNC effects observed. The data were fit directly to the weak spreading width.

For targets with $I^\pi = 0$, the *s*-wave resonances have $1/2^+$ and the *p*-wave resonances $1/2^-$ or $3/2^-$. Only the 1/2 resonances can mix and show parity violation. We assume that the values of the asymmetries measured for different *p*-wave resonances have mean zero and are statistically independent. The likelihood function for several resonances is therefore the product of the individual likelihood functions.

The mean square matrix element M_J^2 is the variance of the distribution of the individual PNC matrix elements $V_{\nu\mu}$. The quantity p_μ in Eq. (5) is a sum of Gaussian random variables $V_{\nu\mu}$ each multiplied by fixed coefficients, and is itself a Gaussian random variable [28]. The variance of p_μ is $(A_\mu M_J)^2$, where

$$A_\mu = \sqrt{\sum_\nu A_{\nu\mu}^2} \quad \text{and} \quad A_{\nu\mu}^2 = \left(\frac{2}{E_\nu - E_\mu}\right)^2 \frac{\Gamma_\nu}{\Gamma_\mu}. \tag{6}$$

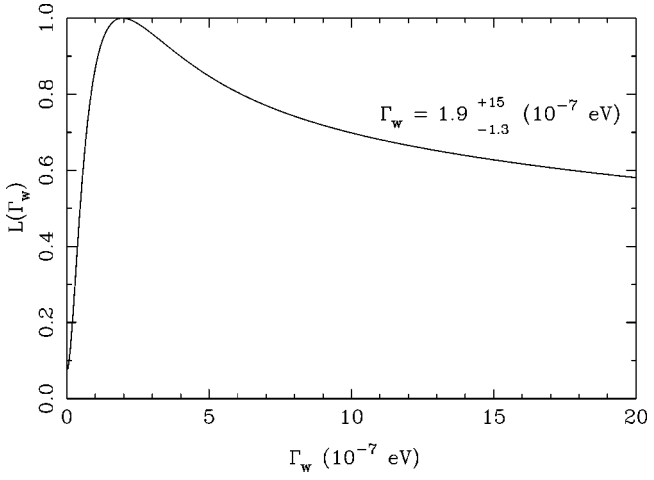

FIG. 6. Likelihood plot for ^{123}Sb. A total of five *p*-wave resonances were analyzed and only one statistically significant PNC effect was observed. The data were fit directly to the weak spreading width. The likelihood plot is extremely broad.

The probability density function of the longitudinal asymmetry p is

$$P(p|M_J A) = \frac{1}{\sqrt{2\pi} M_J A} \exp\left(-\frac{p^2}{2M_J^2 A^2}\right) \equiv G(p,(M_J A)^2), \tag{7}$$

where G represents a Gaussian function.

If the *p*-wave resonance spins are unknown, then one needs two terms, one for the spin 1/2 resonances that can show parity violation and one for the spin 3/2 resonances that cannot show parity violation. If the measurement uncertainty in p is σ_μ, and the *a priori* distribution of the rms matrix element is $P^0(1/2)$, then the likelihood function is

$$L(M_{1/2}) = P^0(1/2) \prod_{\mu=1}^{N} [p(1/2) G(p_\mu, (M_{J=1/2} A_\mu)^2 + \sigma_\mu^2) + p(3/2) G(p_\mu, \sigma_\mu^2)], \tag{8}$$

where the relative probabilities $p(J)$ are estimated using the statistical model.

The problem for $I \neq 0$ targets is much more complicated. For example, ^{121}Sb has $I = 5/2$, and therefore *s*-wave resonances can be formed with spin 2 or 3, while the *p*-wave states can have spins 1, 2, 3, or 4. Only the spin 2 and 3 states can mix and show parity violation.

Suppose that the spins of all *s*-wave resonances are known. If the spin of the *p*-wave level is assumed, then the factor A_μ can be evaluated, but $A_\mu = A_\mu(J)$ depends on the spin assumed because only *s*-wave levels with the same spin as the *p*-wave level mix to produce parity violation. The likelihood function is then obtained by summing over *p*-wave level spins as in the corresponding situation when $I = 0$.

The entrance channel neutron $j = 3/2$ and $j = 1/2$ amplitudes are also unknown. This factor is accounted for statistically by using the average value of the ratio of the $S_{3/2}^1$ and $S_{1/2}^1$ strength functions. The parameter a is defined by $a^2 = S_{3/2}^1 / S_{1/2}^1$. We used $a = 0.65$ for both antimony isotopes and iodine [29].

Due to the level density effect, the rms PNC matrix element may be different for $J = I \pm 1/2$ states. In the absence of spin information we assume that the spreading width is independent of J and fit directly to the spreading width $\Gamma_w = 2\pi (M_J)^2 / D_J$. The likelihood function can be written

$$L(\Gamma_W) = P^0(\Gamma_w) \prod_{\mu=1}^{N} \left[\sum_{J=I\pm 1/2} p(J) P_p^I(p_\mu | M_J A_\mu(J), a, \sigma_\mu) + \sum_{J=I\pm 3/2} p(J) G(p_\mu, \sigma_\mu^2) \right], \tag{9}$$

where M_J should be written as a function of Γ_w. The uncertainties on Γ_w were obtained using the method described by Eadie *et al.* [28]: the confidence interval is determined by solving the equation

TABLE III. Resonance parameters and PNC asymmetries for *p*-wave resonances of ^{127}I.

E (eV)	$g\Gamma_n$ (meV)	A_2 [a] (eV^{-1})	A_3 [a] (eV^{-1})	p (%)	$\lvert p\rvert/\Delta p$
7.51 [b]	0.00012±0.0001	37.6	22.5	0.13±0.14	0.9
10.34 [b]	0.0028±0.0003	9.0	5.2	−0.005±0.03	0.2
13.93 [b]	0.0014±0.0001	15.3	9.0	0.01±0.04	0.3
24.63 [b]	0.00064±0.0006	51.7	19.3	1.65±0.16	10.3
52.20 [b]	0.00085±0.0008	47.8	13.1	0.10±0.18	0.5
53.82	0.019±0.002	8.8	2.9	0.24±0.02	12.0
64.04	0.008±0.001	13.5	6.8	0.06±0.02	3.0
85.84	0.0174±0.002	4.7	13.6	0.24±0.02	11.0
101.1 [b]	0.014±0.002	5.8	6.6	0.10±0.03	3.2
126.0 [b]	0.0021±0.0002	22.3	16.5	−0.48±0.16	3.0
134.1	0.025±0.003	7.9	10.9	0.02±0.02	1.0
136.9 [b]	0.040±0.004	6.8	17.1	0.731±0.016	45.7
145.7	0.033±0.003	10.5	9.0	0.00±0.03	0.0
153.6	0.096±0.003	9.4	2.4	0.01±0.02	0.5
223.4 [b]	0.011±0.001			−0.01±0.13	0.1
256.8	0.052±0.005			0.04±0.04	1.0
274.7 [b]	0.022±0.002			−0.32±0.15	2.1
282.1 [b]	0.0045±0.0005			−0.47±0.53	0.9
352.0	0.088±0.009			−0.539±0.064	8.4
353.3	0.089±0.009			0.05±0.064	0.8

[a]Values above 153.6 eV are not listed; see text for explanation.

[b]New resonances.

$$\ln\left[\frac{L(\Gamma_w^{\pm})}{L(\Gamma_w^{*})}\right]=-\frac{1}{2}, \tag{10}$$

where Γ_w^* is the most likely value and $\Gamma_w^{\pm}$ gives the confidence range.

The likelihood function is not normalizable unless the *prior* tends to zero for large $M_{1/2}$ (or Γ_w). This difference is due to the terms that cannot cause parity violation and lead to a divergent normalization integral. From previous measurements we know that the weak spreading width is unlikely to be more than about 5×10^{-7} eV. For the present calculations we used a constant *prior* below 10×10^{-7} eV and zero above this value.

Note that the expression of Eq. (9) is inconsistent. One should use the weak spreading width as the variable throughout, and transform the *prior* according to $P^0(\Gamma_w)=P^0(M_J(\Gamma_w))dM_J(\Gamma_w)/d(\Gamma_w)$. The change of the argument and the *prior* does not change the final (most likely) value, but does change the corresponding errors because of the nonlinear relationship between the variables M_J and Γ_w. Thus for $I\neq0$, unless there is complete spin information one *must* formulate the problem in terms of the spreading width, and then determine the weak matrix element from the spreading width. This contrasts with the approach for $I=0$, where one determines directly the most likely value of the rms matrix element and then obtains the spreading width.

V. RESULTS AND CONCLUSION

Previous neutron resonance measurements had identified all of the *s*-wave resonances and most of the *p*-wave resonances. All of the newly observed resonances in the three nuclides (five new resonances in ^{121}Sb, one new resonance in ^{123}Sb, and 11 new resonances in ^{127}I) are weak. These resonances are assigned as *p*-wave resonances based on the Bayesian analysis of the neutron widths described in several publications, e.g., [10,13]. The observation of statistically significant PNC effects for three of the new resonances in ^{121}Sb, the one new resonance in ^{123}Sb, and four of the new resonances in ^{127}I is consistent with this assignment. Since there was no information about the *p*-wave spins for any of the three nuclides studied, the likelihood analysis was performed by fitting directly to the weak spreading width.

The resonance parameters and longitudinal asymmetries for ^{121}Sb are listed in Table I. In ^{121}Sb 17 *p*-wave resonances were analyzed below 275 eV and five statistically significant PNC effects were observed. For ^{121}Sb no A_J values are quoted above 170 eV because the spins of many of the *s*-wave resonances are unknown. The likelihood function for ^{121}Sb is shown in Fig. 3. The most likely value of the weak spreading width is $\Gamma_w=4.8^{+8.6}_{-2.9}\times10^{-7}$ eV. The level spacing D_J for ^{121}Sb is 25 eV. From the values for Γ_w and D_J one obtains a weak matrix element $M_J=1.4^{+0.9}_{-0.5}$ meV.

The resonance parameters and longitudinal asymmetries for ^{123}Sb are listed in Table II. The likelihood function for ^{123}Sb is shown in Fig. 4. The most likely value of the weak spreading width is $\Gamma_w=1.9^{+15}_{-1.3}\times10^{-7}$ eV. The level spacing D_J for ^{123}Sb is 60 eV. From the values for Γ_w and D_J one obtains a weak matrix element $M_J=1.3^{+2.7}_{-0.7}$ meV. Since there is only one PNC effect the likelihood function is

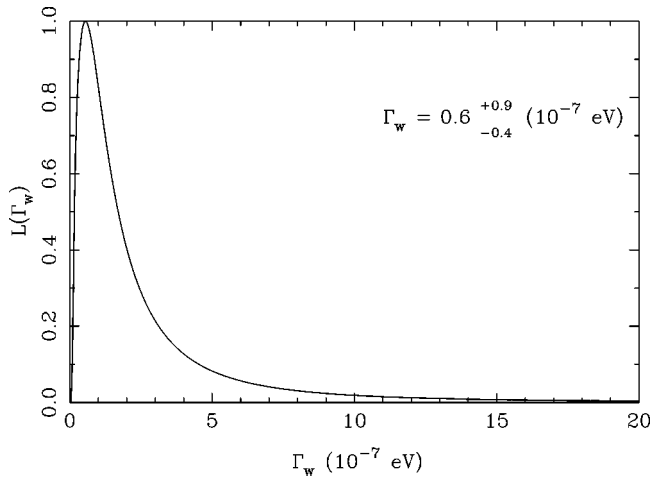

FIG. 7. Likelihood plot for ^{127}I. A total of 20 *p*-wave resonances were analyzed and eight statistically significant PNC effects were observed. The data were fit directly to the weak spreading width.

broader and the resulting values for the spreading width and the weak matrix element have larger uncertainties.

The resonance parameters and longitudinal asymmetries for ^{127}I are listed in Table III. For iodine a total of 20 *p*-wave resonances were analyzed. Since above 220 eV the spins of the *s*-wave resonances are unknown, no A_J values are quoted above this energy. The likelihood function for ^{127}I is shown in Fig. 7. The most likely value of the weak spreading width is $\Gamma_w = 0.6^{+0.9}_{-0.4} \times 10^{-7}$ eV. The level spacing D_J for ^{127}I is 23 eV. From the values for Γ_w and D_J one obtains a weak matrix element $M_J = 0.5^{+0.3}_{-0.2}$ meV.

The values of the weak spreading widths and the weak matrix elements are consistent with those observed in other nuclei. If all of the data measured by the TRIPLE Collaboration are considered, one obtains an average value of $\Gamma_w = 1.8^{+0.3}_{-0.3} \times 10^{-7}$ eV [6]. The present results agree well with the existing data. Overall the PNC measurements are consistent with a (global) constant value for the weak spreading width. However, there is evidence that there are local fluctuations. For example, ^{133}Cs has an anomalously low value of the weak spreading width [9].

ACKNOWLEDGMENTS

This work was supported in part by the U.S. Department of Energy, Office of High Energy and Nuclear Physics, under Grant Nos. DE-FG02-97-ER41042 and DE-FG02-97-ER41033, and by the U.S. Department of Energy, Office of Energy Research, under Contract No. W-7405-ENG-36.

[1] V. P. Alfimenkov, S. B. Borzakov, Vo Van Thuan, Yu. D. Mareev, L. B. Pikelner, A. S. Khrykin, and E. I. Sharapov, Nucl. Phys. **A398**, 93 (1983).
[2] J. D. Bowman, G. T. Garvey, Mikkel B. Johnson, and G. E. Mitchell, Annu. Rev. Nucl. Part. Sci. **43**, 829 (1993).
[3] C. M. Frankle, S. J. Seestrom, N. R. Roberson, Yu. P. Popov, and E. I. Sharapov, Phys. Part. Nucl. **24**, 401 (1993).
[4] V. V. Flambaum and G. F. Gribakin, Prog. Part. Nucl. Phys. **35**, 423 (1995).
[5] G. E. Mitchell, J. D. Bowman, and H. A. Weidenmüller, Rev. Mod. Phys. **71**, 445 (1999).
[6] G. E. Mitchell, J. D. Bowman, S. I. Penttilä, and E. I. Sharapov, Phys. Rep. (to be published).
[7] S. L. Stephenson *et al.*, Phys. Rev. C **58**, 1236 (1998).
[8] B. E. Crawford *et al.*, Phys. Rev. C **58**, 1225 (1998).
[9] E. I. Sharapov *et al.*, Phys. Rev. C **59**, 1131 (1999).
[10] D. A. Smith *et al.*, Phys. Rev. C **60**, 045502 (1999).
[11] L. Y. Lowie *et al.*, Phys. Rev. C **59**, 1119 (1999).
[12] S. J. Seestrom *et al.*, Phys. Rev. C **58**, 2977 (1998).
[13] S. L. Stephenson *et al.*, Phys. Rev. C **61**, 045501 (2000).
[14] E. I. Sharapov *et al.*, Phys. Rev. C **59**, 1772 (1999).
[15] S. J. Seestrom *et al.*, Nucl. Instrum. Methods Phys. Res. A **433**, 603 (1999).
[16] P. W. Lisowski, C. D. Bowman, G. J. Russell, and S. A. Wender, Nucl. Sci. Eng. **106**, 208 (1990).
[17] N. R. Roberson *et al.*, Nucl. Instrum. Methods Phys. Res. A **326**, 549 (1993).
[18] J. J. Szymanski *et al.*, Nucl. Instrum. Methods Phys. Res. A **340**, 564 (1994).
[19] S. I. Penttilä, J. D. Bowman, P. P. J. Delheij, C. M. Frankle, D. G. Haase, H. Postma, S. J. Seestrom, and Yi-Fen Yen, in *High Energy Spin Physics*, edited by K. J. Heller and S. L. Smith (AIP, New York, 1995), p. 532.
[20] J. D. Bowman, S. I. Penttilä, and W. B. Tippens, Nucl. Instrum. Methods Phys. Res. A **369**, 195 (1996).
[21] Yi-Fen Yen *et al.*, Nucl. Instrum. Methods Phys. Res. A **447**, 476 (2000).
[22] J. D. Bowman, Y. Matsuda, Yi-Fen Yen, and B. E. Crawford (unpublished).
[23] C. W. Reich and M. S. Moore, Phys. Rev. **111**, 929 (1958).
[24] P. F. Rose, BNL-NCD-17541, 1991.
[25] T. Nakagawa *et al.*, J. Nucl. Sci. Technol. **32**, 1259 (1995).
[26] V. W. Yuan *et al.*, Phys. Rev. C **44**, 2187 (1991).
[27] J. D. Bowman, L. Y. Lowie, G. E. Mitchell, E. I. Sharapov, and Yi-Fen Yen, Phys. Rev. C **53**, 285 (1996).
[28] W. T. Eadie, P. Drijard, F. E. James, M. Roos, and B. Sadoulet, *Statistical Methods in Experimental Physics* (North Holland, Amsterdam, 1971), p. 204.
[29] L. V. Mitsyna, A. B. Popov, and G. S. Samosvat, *Nuclear Data for Science and Technology*, edited by S. Igarasi (Saikon, Tokyo, 1988), p. 111.